Journal of the European Ceramic Society 7 (1991) 197–206

The System Y_2O_3–Sc_2O_3–ZrO_2: Phase Stability and Ionic Conductivity Studies

F. T. Ciacchi & S. P. S. Badwal

CSIRO, Division of Materials Science and Technology, Normanby Road, Locked Bag 33, Clayton 3168, Victoria, Australia

(Received 16 July 1990; revised version received 31 October 1990; accepted 5 November 1990)

Abstract

The ionic conductivity of the system Y_2O_3–Sc_2O_3–ZrO_2 has been investigated, as a function of temperature (400–1000°C) and time (at 1000°C), for a range of Y/Sc ratios (eight compositions) at a constant dopant level of 8 mol%. The conductivity of scandia-rich compositions was almost twice that of the fully stabilized Y_2O_3–ZrO_2 but in all the specimens the conductivity deteriorated with time on annealing at 1000°C. In Sc_2O_3-rich compositions, a dopant-rich t'-phase is formed by diffusionless transformation from the cubic phase on cooling the ceramic from the sintering temperature. On annealing at 1000°C, this phase decomposes to low-dopant t-ZrO_2 precipitates and a cubic zirconia solid-solution matrix. In Y_2O_3-rich compositions only the cubic phase is formed but this is not an equilibrium phase with respect to dopant distribution. On annealing a slight redistribution of the dopant level and precipitation of t-ZrO_2 takes place. These changes in the microstructure are responsible for the observed conductivity ageing process. The decrease in the conductivity and increase in the activation energy with increasing Y_2O_3 above 850°C has been discussed in terms of the steric blocking effect of the larger Y^{3+} cation.

Im Dreistoffsystem Y_2O_3–Sc_2O_3–ZrO_2 wurde die Ionenleitfähigkeit in Abhängigkeit der Temperatur (400–1000°C) und der Zeit (bei 1000°C) für verschiedene Y/Sc-Verhältnisse (acht Zusammensetzungen) bei einem gleichbleibenden Gehalt an Dotierstoffen von 8 mol% untersucht. In den Sc_2O_3-reichen Zusammensetzungen war die Leitfähigkeit nahezu doppelt so hoch als in voll stabilisiertem Y_2O_3–ZrO_2. Die Leitfähigkeit nahm jedoch in allen Proben bei einer Glühbehandlung bei 1000°C im Lauf der Zeit ab. In Sc_2O_3-reichen Zusammensetzungen bildet sich beim Abkühlen von der Sintertemperatur aus der kubischen Phase durch eine diffusionslose Umwandlung eine hoch dotierte t'-Phase. Beim Glühen bei 1000°C zersetzt sich diese Phase zu niedrig dotierten t-ZrO_2-Teilchen in einer Matrix aus einem kubischen Mischkristall. In Y_2O_3-reichen Zusammensetzungen bildet sich nur die kubische Phase. Diese ist jedoch im Sinne der Verteilung der Dotieratome nicht im Gleichgewicht. Eine Glühbehandlung hat eine geringfügige Umverteilung der Dotieratome und die Ausscheidung von t-ZrO_2 zur Folge. Diese Gefügeveränderungen sind für den beobachteten Alterungsprozeß der Ionenleitfähigkeit verantwortlich. Die Abnahme der Leitfähigkeit und die höhere Aktivierungsenergie mit zunehmendem Y_2O_3-Anteil über 850°C wird auf eine sterisch bedingte blockierende Wirkung des grösseren Y^{3+}-Kations zurückgeführt.

On a étudié la conductivité ionique du système Y_2O_3–Sc_2O_3–ZrO_2 en fonction de la température (400–1000°C) et du temps (à 1000°C), pour une gamme de rapports Y/Sc (huit compositions) et à une teneur en dopant constante de 8% molaires. La conductivité des compositions riches en oxyde de scandium était presque deux fois plus élevée que celle de Y_2O_3–ZrO_2 totalement stabilisée, mais tous les échantillons présentaient une détérioration de la conductivité en fonction du temps lors du recuit à 1000°C. Dans les compositions riches en Sc_2O_3, une phase t' riche en dopant se formait par transformation non diffusionnelle à partir de la phase cubique lors du refroidissement de la céramique à partir de sa température de frittage. Lors d'un recuit à 1000°C, cette phase se décompose en des précipités de t-ZrO_2 pauvres en dopant dans une matrice de solution solide de zircone

Journal of the European Ceramic Society 0955-2219/91/$3.50

cubique. Dans le cas de compositions riches en Y_2O_3 la phase cubique était seule à se former mais il n'y avait pas d'équilibre de phase par rapport à la distribution du dopant. Le recuit permet une légère redistribution du dopant et provoque la précipitation de t-ZrO_2. Ces changements de microstructure sont reponsables du phénomène de vieillissement de conductivité observé. On explique la décroissance de la conductivité et l'augmentation de l'énergie d'activation avec l'accroîssement de Y_2O_3 au dessus de 850°C par l'effet de blocage stérique des ions Y^{3+} de grande dimension.

1 Introduction

One of the major areas of applications for zirconia (ZrO_2) based ceramics is that as a solid electrolyte in electrochemical devices. The oxygen-ion conducting property of solid electrolyte cells plays an important role for measuring the thermodynamic and kinetic properties of oxygen-bearing systems.[1-3] Several different types of oxygen sensors have been developed for the monitoring and control of combustion processes in furnaces, boilers, automotive exhausts, for process control in chemical and metallurgical industries and for the control and reduction of pollutant emissions.[4,5] Zirconia-based ceramics have the potential to revolutionize future power generation. In this regard significant advances have already been made on the development of solid oxide fuel cells.[6] Similar cells can also be used as oxygen pumps, electrochemical reactors and for the production of hydrogen.[7,8]

In a quest for a better conducting solid electrolyte, a ternary oxide system Y_2O_3–Sc_2O_3–ZrO_2 has been investigated. In a previous paper[9] the phase assemblage in the ternary system was reported as a function of the Sc_2O_3/Y_2O_3 ratio (eight compositions) for a constant dopant level of 8 mol%. In this paper the results of conductivity measurements as a function of time and temperature are reported. These investigations were carried out with impedance spectroscopy and a four-probe DC technique and have been combined with previously reported phase assemblage studies to understand the ageing behaviour in the system.

2 Experimental Procedure

The details of specimen preparation, nomenclature, measured and calculated densities and phase assemblage have been reported in a previous paper.[9] In summary, specimens S1–S8, R3, R5 and AS1–AS8 were prepared by co-precipitation (S1 to S8, R3, R5: as sintered and AS1 to AS8: after annealing at 1000°C for 2000 h), followed by milling the powder in a plastic (R3, R5) or a glass-bonded (S1–S8) teflon container, calcination, pressing into bars and sintering. Table 1 gives some preparation details along with average grain sizes.

Impedance measurements were performed on all as-sintered and annealed specimens (dimensions: thickness = 3·1–3·5 mm, a = 6·3–7·3 mm and b = 7·1–7·6 mm) over the frequency range 5 Hz–10 MHz with a HP 4192A impedance analyser. The electrodes used were either a commercially available platinum paste 6082 (Engelhard Industries) or a low-impedance electrode consisting of 75 wt% $(U_{0.38}Sc_{0.62})O_{2\pm x}$ (a fluorite-type solid solution) and 25 wt% PtO_2 (PtU2B).[10] The temperature range for the measurements was between 325 and 600°C and the data were recorded during the cooling cycle (at 50°C intervals from 600 to 450°C and 25°C intervals from 450 to 325°C). The cell was initially left at 600°C for 6 h and then after each temperature change the cell was allowed to settle for 90 min before recording data.

A four-probe DC conductivity technique was used to measure the total ionic conductivity of all as-sintered specimens (S1–S8, R3, R5) as a function of

Table 1. Details of specimen preparation[a]

Specimen	*Specimen composition*[b] *(x mol% Y_2O_3)*	*Calcination temperature (T, °C)*[c]	*Sintering temperature (T, °C)*[d]
S1	1	700	1 750
S2	2	700	1 750
S3	3	700	1 750
S4	4	700	1 750
S5	5	700	1 750
S6	6	700	1 750
S7	7	700	1 750
S8	8	700	1 750
R3	3	700	1 750
R5	5	700	1 750
AS1	1	—	—[e]
AS2	2	—	—[e]
AS3	3	—	—[e]
AS4	4	—	—[e]
AS5	5	—	—[e]
AS6	6	—	—[e]
AS7	7	—	—[e]
AS8	8	—	—[e]

[a] Average grain size (μm ± 2·5): 28 (S1), 25 (S2), 32 (S3), 27 (S4), 33 (S5), 39 (S6), 35 (S7), 38 (S8).
[b] x mol% Y_2O_3 in x mol% Y_2O_3 + (8-x) mol% Sc_2O_3 + 92 mol% ZrO_2.
[c] For 1 h.
[d] For 15 h.
[e] Coprecipitated and sintered specimens S1–S8 after annealing at 1000°C for 2000 h. The composition as per S1–S8 respectively. The prefix 'A' indicates annealing.

temperature (395–1000°C) and time (at 1000°C). No measurements were made on specimens which had undergone an additional heat treatment at 1000°C for 2000 h. Instead, conductivity for each as-sintered specimen was monitored as a function of time at the annealing temperature of 1000°C. Specimens were in the form of bars with typical dimensions $a = 3{\cdot}1$–$3{\cdot}5$ mm, $b = 6{\cdot}3$–$7{\cdot}3$ mm and length 19·9–20·1 mm. Potential probe grooves around the specimen bar (approximately 4 mm from each end of the bar) were made and 13%Rh-Pt wire was wedged in the grooves around the specimens. Current probes were constructed by applying a thick layer of platinum paste 6082 or PtU2B to each end of the specimen bar. The furnace constant temperature zone was 5 cm long (within 1°C). The currents passed varied between 100 nA (at low temperatures) to 2 mA (at high temperatures), depending upon the specimen resistance. The voltage signal across potential probes was measured with either a digital voltmeter (input impedance of 10^{10} ohm) or an electrometer (input impedance of 10^{14} ohm). The details of this technique will be described in a separate publication.[11]

The majority of DC conductivity measurements were made over the temperature range 395–1000°C at 15–25°C temperature intervals for two heating and cooling cycles. About 30–45 min were given after each temperature change before recording data. After the temperature had reached 1000°C the data were recorded at this temperature as a function of time at regular intervals for a total of 9500 min at the end of the first heating cycle and 5200 min at the end of the second heating cycle. In some cases the conductivity bars, after measurements as a function of temperature and time, were given heat treatment at 1700°C and the conductivity measurement procedure repeated to check if the effect of ageing could be reversed.

3 Results and Interpretation

3.1 Impedance studies

In general two arcs were observed for the electrolyte behaviour in the impedance plane. In the following impedance diagrams the arc on the right is due to the grain boundary and the arc on the left is due to the volume resistivity, Z′ is the real and Z″ is the imaginary part of the impedance. The impedance data were analysed by nonlinear least squares analysis programs.

In general, the contribution of the grain boundary resistivity was small except for specimens S3 and S5.

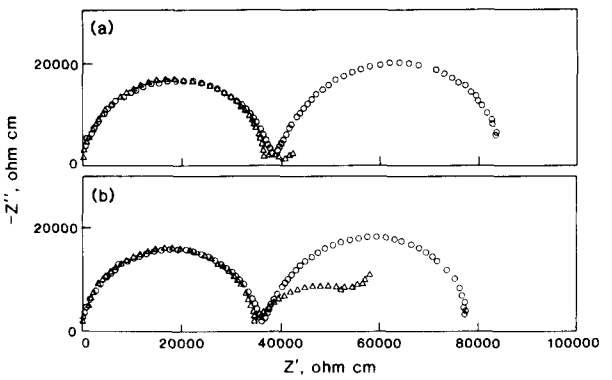

Fig. 1. Impedance plots at 350°C of: (a) 3 mol% Y_2O_3 + 5 mol% Sc_2O_3 + 92 mol% ZrO_2 (S3, R3) and (b) 5 mol% Y_2O_3 + 3 mol% Sc_2O_3 + 92 mol% ZrO_2 (S5, R5) with ○, high (S3, S5) and △, low (R3, R5) grain boundary impurity phase.

This seems to have resulted from contamination from the glass-bonded teflon container. When these two specimens were prepared by milling the coprecipitated powder in a plastic container the grain boundary resistivity decreased significantly (Fig. 1).

Annealing at 1000°C for 2000 h lead to an increase in both the grain boundary and the volume resistivity as shown in Figs 2 and 3 although the effect of annealing was more pronounced on the volume resistivity. At low temperatures the volume resistivity increased with increase in the yttria content (Fig. 4). This behaviour was more dominant in annealed specimens. Table 2 gives activation energy values for the volume resistivity in the low temperature range (325–425°C). The activation energy decreased with increasing yttria content for both as-sintered and annealed specimens. Annealing had little effect on the activation energy except for compositions with higher yttria content (≥ 6 mol%) for which a slight increase was observed.

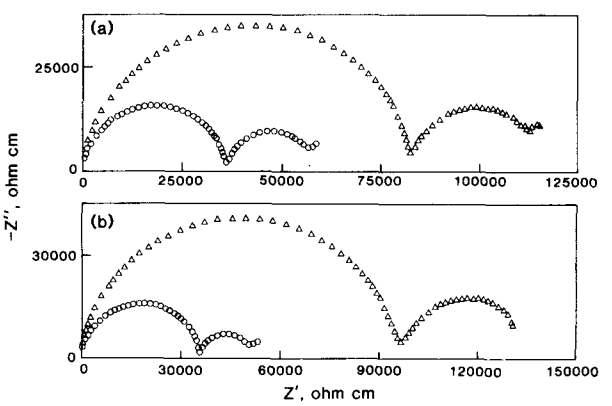

Fig. 2. Impedance plots at 350°C of: (a) 2 mol% Y_2O_3 + 6 mol% Sc_2O_3 + 92 mol% ZrO_2 and (b) 4 mol% Y_2O_3 + 4 mol% Sc_2O_3 + 92 mol% ZrO_2. ○, As-sintered: △, annealed specimens.

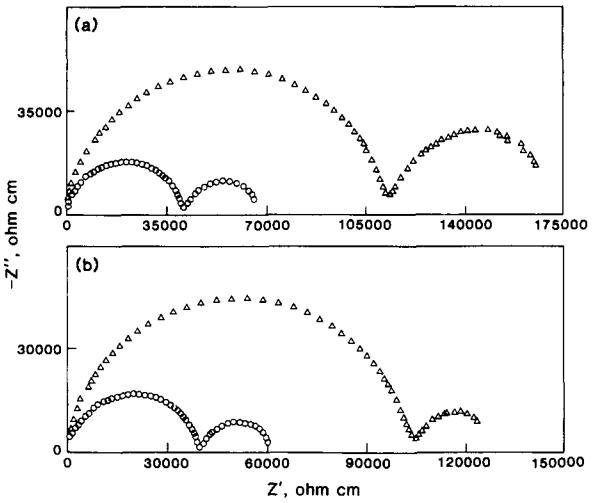

Fig. 3. Impedance plots at 350°C of: (a) 6 mol% Y_2O_3 + 2 mol% Sc_2O_3 + 92 mol% ZrO_2 and (b) 8 mol% Y_2O_3 + 92 mol% ZrO_2. ○, As-sintered; △, annealed specimens.

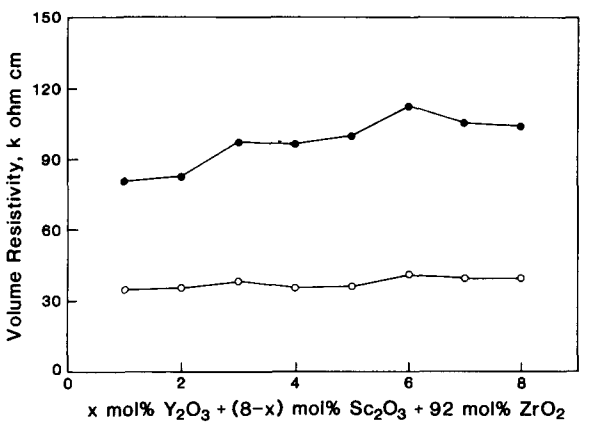

Fig. 4. Plots of volume resistivity as a function of composition at the measurement temperature of 350°C. ○, As-sintered; ●, annealed specimens.

Table 2. Activation energies of various specimens from impedance data in the low temperature region (325–425°C)

Specimen	*Activation energy ($kJ\,mol^{-1}$)[a] for the volume resistivity*
S1	119 ± 1
S2	114 ± 2
S3	110 ± 1
S4	109 ± 1
S5	108 ± 1
S6	106 ± 1
S7	103 ± 1
S8	98 ± 1
R3	110 ± 1
R5	107 ± 1
AS1	118 ± 2
AS2	112 ± 2
AS3	110 ± 2
AS4	109 ± 2
AS5	110 ± 1
AS6	108 ± 1
AS7	108 ± 1
AS8	105 ± 1

[a] Calculated from $\sigma T = A \exp(-E_a/RT)$.

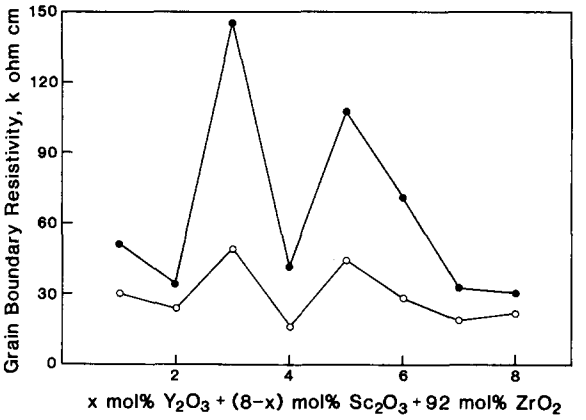

Fig. 5. Plots of grain boundary resistivity as a function of composition at the measurement temperature of 350°C. ○, As-sintered; ●, annealed specimens.

Figure 5 shows the grain boundary resistivity as a function of composition for as-sintered and annealed materials at 350°C. In general, materials which had the higher grain boundary resistivity before annealing, especially specimens S3, S5 and S6, showed the largest increase on annealing at 1000°C for 2000 h.

It is not obvious why the grain boundary resistivity increased as a consequence of the anneal. Possible causes may be associated with segregation of the dopant at the grain boundaries leading to changes in the chemical composition of the grain boundary phase, or relocation or a more uniform 'wetting' of grains by the glassy phase.

3.2 Four-probe DC technique

3.2.1 Effect of time

The effect of the annealing temperature on the conductivity change was studied on a pure scandia–zirconia (7·8 mol% $Sc_2O_3 + ZrO_2$) composition from the previous study[12] also prepared by the coprecipitation technique. As shown in Fig. 6, after

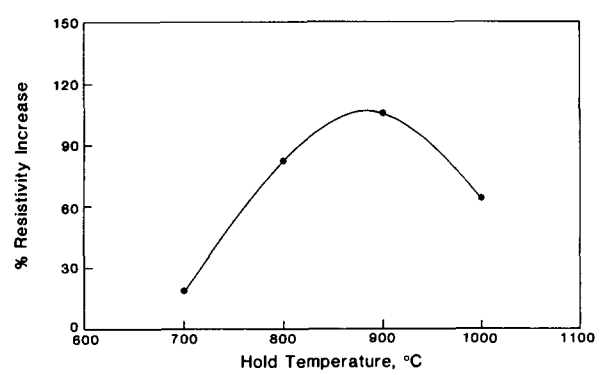

Fig. 6. Percentage resistivity increase for 7·8 mol% Sc_2O_3 + 92·2 mol% ZrO_2 after 9500 min anneal as a function of hold temperature.

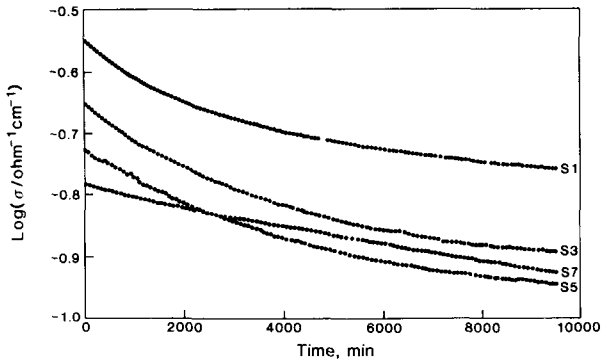

Fig. 7. Plots of conductivity versus time at 1000°C for the as-sintered specimens S1, S3, S5 and S7.

9500 min anneal at each temperature, the maximum percentage resistivity increase was observed when the specimen was held at about 900°C. In the present study, for convenience, the effect of annealing was studied at 1000°C, the maximum measurement temperature.

The conductivity of all as-sintered compositions deteriorated with time at 1000°C. Initially a sharp and then a slow but continuous decrease in conductivity with time was observed, as shown in Fig. 7 for some specimens for the anneal (1000°C) at the end of first heating cycle. The rate of change of the conductivity in the early stages of the anneal was maximum for the highest scandia-containing composition (S1) and the rate, in general, decreased with increasing yttria content.

Figure 8 shows variation in conductivity as a function of the yttria content before (within 5 min of the temperature reaching 1000°C) and after annealing at 1000°C for 9500 and 14 700 min. After the 9500 min anneal the conductivity had decreased by about 30–80% (depending upon the specimen composition); the lowest change occurring in a specimen with the highest yttria content (S8). At the

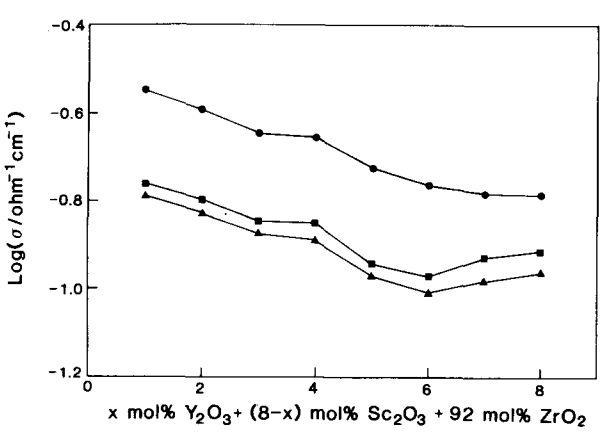

Fig. 8. Total conductivity versus composition plots at 1000°C at different stages of anneal. ●, 5 min; ■, 9500 min; ▲, 14 700 min.

end of the second heating cycle, maintaining the temperature at 1000°C for a further 5200 min had little effect on the conductivity. The effect of ageing was reversed when the specimens were given heat treatment at 1700°C (a temperature in the cubic-phase field) and the pre-anneal conductivity was restored.

3.2.2 Effect of temperature

Arrhenius plots for all the specimens studied (S1–S8, R3 and R5) demonstrated a continuous change in the slope towards a lower activation energy with increasing temperature (Fig. 9) both before and after annealing at 1000°C. The activation energy values in the low (395–500°C) and high (850–1000°C) temperature ranges were determined from the relationship:

$$\sigma T = A \exp(-E_a RT)$$

and are given in Table 3 (σ = conductivity, T = temperature in Kelvin, A = pre-exponential term, E_a = activation energy, and R = gas constant). They consist of contributions from both the grain boundary and the volume resistivity. The activation energy in the high temperature range, for the first heating cycle, is lower by about 5–10 kJ mol^{-1} when compared with the subsequent cycles. The difference can be explained in the following way. With increasing temperature, the conductivity increases. However, above about 700°C, annealing of specimens leading to a decrease in the conductivity, is expected to occur mainly during the first heating cycle. This would counteract the normal effect of temperature on conductivity giving rise to an artificial slope and a lower activation energy value than that would have been obtained in the absence of any annealing. Another minor possibility is the enrichment of the matrix with the dopant as a result of annealing[9] which can also lead to a slight increase

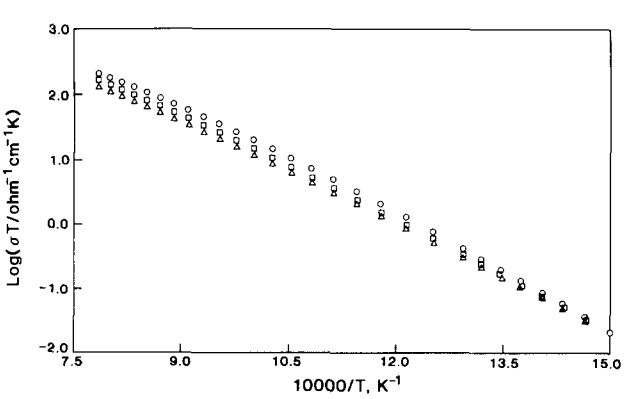

Fig. 9. Arrhenius plots for the second cooling cycle of specimens: ○, S1; □, S4; △, S7.

Table 3. Activation energies of various specimens for low and high temperature regions

Specimen	*Activation energy* ($kJ\,mol^{-1} \pm 3\,kJ\,mol^{-1}$)		
	Low temperature region[a] *(395–500°C)*	*High temperature region (850–1000°C)*	
		H1[b]	*C1, H2, C2*[b]
S1	119	78	85
S2	116	77	86
S3	114	86	98
S4	111	80	89
S5	112	90	97
S6	110	83	93
S7	108	82	90
S8	107	85	89
R3	112	74	84
R5	109	81	87[c]

Activation energy calculated from $\sigma T = A \exp(-E_a/RT)$.
[a] Average of all cycles.
[b] H1, For first heating cycle only; C1, H2, C2, average of first cooling, second heating and second cooling cycles.
[c] First cooling cycle only.

in the activation energy.[13] For this reason, in the high temperature range, the activation energy for the first heating cycle is given separately from the average of the remaining cycles.

For the low temperature range (395–500°C), no appreciable differences were observed between the activation energy values of various cycles. The activation energy (average of all cycles for a specimen) was only slightly higher than that determined for the volume conductivity from impedance studies (in general within 5 kJ mol^{-1}) but it was about 15–35 kJ mol^{-1} higher than that in the high temperature range. Figure 10 shows plots of activation energy as a function of specimen composition. In the low temperature range, the activation energy decreased with increasing yttria content whereas in the high temperature range it increased with increasing yttria concentration.

The best conductivity was observed for the highest Sc_2O_3-containing material at 1000°C and it decreased monotonically as the Y_2O_3/Sc_2O_3 ratio increased (Fig. 8).

3.2.3 Effect of impurity phase on the total conductivity

Arrhenius plots for the first heating cycle of the two compositions, 3 mol% Y_2O_3 + 5 mol% Sc_2O_3 + 92 mol% ZrO_2 and 5 mol% Y_2O_3 + 3 mol% Sc_2O_3 + 92 mol% ZrO_2 either (a) milled in a glass-bonded teflon container (S3 and S5) or (b) milled in a plastic container (R3 and R5) respectively are shown in Fig. 11.

Although specimens with high impurity content had low conductivity at lower temperatures, this was not the case at higher temperatures. For example, specimens S3 or S5 (high impurity content) had much lower conductivity at low temperatures (Fig. 11) than the corresponding specimen R3 or R5 (low impurity content) but the glassy impurities had little effect on the initial (pre-anneal) conductivity at 1000°C. Conductivity values measured soon after temperature reached 1000°C were comparable for low and high impurity specimens for the respective compositions. However, the conductivity deterioration at 1000°C was observed to be higher for the S3 specimen compared with the R3 specimen. This suggests that the grain boundary glassy-phase impurity has a negligible contribution on the conductivity of the material at 1000°C (before the anneal) but has a significant role in its deterioration as a consequence of the anneal.

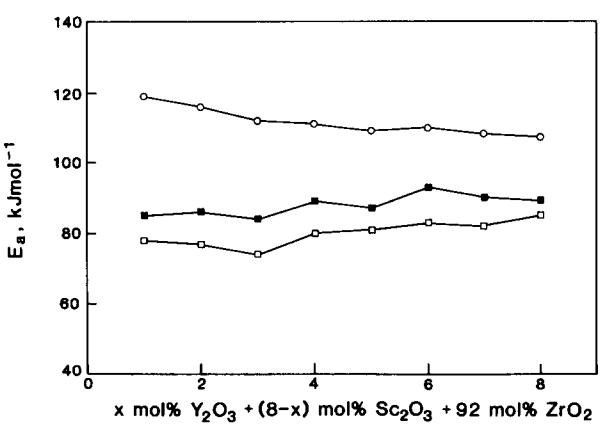

Fig. 10. Activation energy for the total conductivity as a function of specimen composition for low and high temperature regions. ○, Low temperature region (average of all cycles); □ and ■, high temperature region: □, first heating cycle; ■, average of remaining cycles.

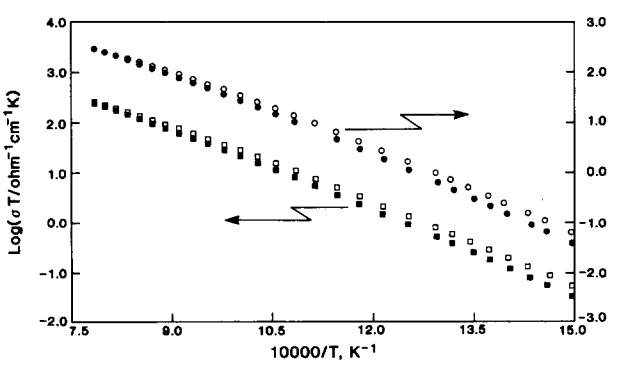

Fig. 11. Arrhenius plots for the first heating cycle of two 3 mol% Y_2O_3 + 5 mol% Sc_2O_3 + 92 mol% ZrO_2 (● and ○) and 5 mol% Y_2O_3 + 3 mol% Sc_2O_3 + 92 mol% ZrO_2 (■ and □) compositions milled in a glass-bonded teflon (● and ■) and a plastic (○ and □) container.

4 Discussion

The most significant results from the previous sections are summarized as follows:

(i) On annealing at 1000°C, the conductivity deteriorated with time for all compositions, the highest percentage change occurring for the specimen with the highest scandia content.
(ii) The conductivity of annealed (at 1000°C) specimens was restored if the material was given a heat treatment at 1700°C (a temperature in the cubic-phase field) removing the effects of annealing at 1000°C and changes which may have occurred during heating and cooling.
(iii) At 1000°C the best conductivity was observed for the highest scandia-containing composition and it decreased monotonically as the yttria/scandia ratio increased.
(iv) Conductivity as a function of temperature showed a continuous change in slope towards a lower activation energy with increasing temperature regardless of whether specimens were annealed or not.
(v) The activation energy in the high temperature range (850–1000°C) increased with increasing yttria content whereas in the low temperature range (395–500°C (four-probe DC data) and 325–425°C (impedance data)) it decreased with increasing yttria content.
(vi) The effect of impurities and the grain boundary resistivity was more predominant at lower temperature but it decreased with increasing temperature. At around 1000°C the major contribution to the total resistivity appears to come from the volume resistivity.

4.1 Effect of impurities

All the specimens studied showed contributions from both grain boundary and volume resistivities low temperatures. The contribution from the grain boundary to the total resistivity, in particular, was much higher for specimens which had a high impurity content but the same dopant composition. It is well known that glassy impurities in zirconia-based ceramics segregate at grain boundaries during sintering. The nature and location of these impurity phases, which is a function of the sintering conditions and post-sinter heat treatments in addition to the level and type of impurities present in the starting powders, have major influences on the grain boundary resistivity. The impurity phases, in general, are low conducting and therefore can partially or completely block the paths of migrating oxygen ions.

Although the grain boundary resistivity made a significant contribution to the total resistivity at lower temperatures, its effect at higher temperatures (around 1000°C) was relatively small (Fig. 11). This is consistent with the observations of Kleitz *et al.*[14] who suggested that the temperature at which the blocking effect (grain boundary resistivity) vanishes depends on the level of sample purity. According to these authors the temperature at which the grain boundary resistivity influence disappears can vary from ~700°C for nominally pure materials to as much as 1000°C for technical-quality materials. The diminishing contribution of the grain boundary to the total resistivity with increasing temperature was also confirmed in this laboratory where measurements on two materials of 3 mol% Y_2O_3–ZrO_2 composition, one of high purity and the other containing a large impurity phase, were made. The material with higher impurity content had much higher contribution from the grain boundary resistivity and its total resistivity compared with that of the high purity material was higher by a factor of 6 at 400°C but only by a factor of 1·3 at 1000°C.

Badwal[15] states that the activation energy for the volume resistivity, although somewhat comparable at low temperatures, is considerably lower at high temperatures compared with the activation energy of the grain boundary resistivity. Thus, with increasing temperature the relative contribution of the grain boundary resistivity is expected to decrease with temperature. However, in materials with large impurity content the contribution of the grain boundary resistivity may not decrease sufficiently and therefore may influence the activation energy in the high temperature range. This indeed was reflected in the slightly higher activation energy (high temperature region) observed for specimens S3 and S5 compared with R3 and R5 respectively.

4.2 Ageing

In general, the observed ageing behaviour (isothermal increase in the conductivity with time) in zirconia-based solid electrolytes can be attributed to three major possible causes.[16] The type of ageing behaviour, the ageing rate and intensity of ageing are determined by the temperature and the electrolyte composition.

(i) For single-phase materials the main cause of ageing is the formation and growth of fine microdomains or ordered phases.

(ii) For materials which are annealed in the two-phase region, the ageing can be attributed to solute redistribution and resulting precipitation and growth of the low conducting phases. The ageing process in this case is determined by the kinetics of two processes running independently of each other associated with the growth of a number of second-phase centres and precipitate growth.

(iii) In polycrystalline materials with significant levels of impurities, in addition to the change in the bulk resistivity a change in the grain boundary contact resistivity has also been observed.

The present conductivity results are consistent with this general interpretation if they are combined with the results of phase assemblage studies reported in a previous publication.[9] All the compositions of the ternary oxide system investigated here were sintered in the cubic-phase field. In scandia-rich compositions between 7 mol% Sc_2O_3 + 1 mol% Y_2O_3 + 92 mol% ZrO_2 (S1) and 3 mol% Sc_2O_3 + 5 mol% Y_2O_3 + 92 mol% ZrO_2 (S5) inclusive, a dopant-rich tetragonal (t') phase is formed as a result of displacive or diffusionless transformation of the cubic phase on cooling the materials from the sintering temperature.

The t'-phase is metastable in nature and on annealing at 1000°C decomposes into a cubic zirconia solid-solution matrix and low conducting t-ZrO_2 precipitates. This process requires diffusion and distribution of the stabilizing cations and takes place over a period of time. This should ideally lead to the formation of an equilibrium cubic phase with dopant content higher than that of the corresponding t'-phase. However, in the scandia–zirconia system, because of the intrinsic slowness of the phase reactions, the products of decomposition of the metastable phase themselves may be nonequilibrium phases. It is possible that high scandia-content ordered phases (similar to those in the MgO–ZrO_2 system[17]) with low conductivity are formed, thus isolating some conducting phase regions from the conducting paths. Moreover, significant compositional variations with respect to the dopant level can occur in such a system. The change in conductivity for specimens S1–S5 is therefore related to the rate at which this process proceeds. Conductivity results at 1000°C as a function of time can be interpreted in terms of the rate of decomposition of the t'-phase. From phase assemblage studies on as-sintered and annealed materials[9] it was clearly obvious that although the t'-phase was present in the as-sintered specimens, the annealed materials consisted mainly of the cubic phase with t-ZrO_2 precipitates dispersed in it.

In the yttria-rich as-sintered compositions S6, S7 and S8, the t'-phase is not formed. Instead the high-temperature cubic phase is retained when these materials are cooled from the sintering temperature. This phase, like the t'-phase, is also not in an equilibrium state with respect to dopant distribution. On annealing these specimens at 1000°C, a redistribution of the dopant level and precipitation of t-ZrO_2 takes place, as determined by equilibrium phase boundaries. This was supported by the small but consistent increase in the cell volume observed for the cubic phase and precipitate (t-ZrO_2) appearance and growth on annealing (X-ray diffraction and TEM studies[9]). The change in conductivity with time for these specimens is related to this process. The conductivity results strongly support the phase diagrams proposed by Scott,[18] Stubican *et al.*[19] and Thornber *et al.*[20]

The heat treatment of the annealed specimens in the cubic-phase field restores the system pre-anneal conductivity and the phase assemblage.

Some previous authors[21,22] have reported a decrease in the conductivity of 8–9 mol% Sc_2O_3–ZrO_2 compositions with time. Their results were interpreted in terms of precipitation of the β-phase (an ordered, low-conducting rhombohedral phase with Sc_2O_3 content in the vicinity of 12·73 mol%[20]). The nature of the ageing process in their specimens is somewhat uncertain, as the specimens were prepared by mixing oxides and dopant inhomogeneities are likely to be present. Badwal[12] performed ageing experiments on several Sc_2O_3–ZrO_2 compositions prepared by the coprecipitation technique and found no evidence of the β-phase. The β-phase was detected only in specimens prepared by mixing oxide powders and which had not fully reacted. In the present case all specimens were prepared by the coprecipitation technique and no inhomogeneous distribution of dopants or the presence of the β-phase was observed in as-sintered or annealed specimens.

4.3 Effect of Sc_2O_3/Y_2O_3 ratio on conductivity and activation energy

Despite some uncertainty created by the complex phase assemblage, a number of trends consistently observed both in as-sintered and annealed specimens need further discussion. For example, (i) the conductivity in the ternary system decreased monotonically with increasing yttria content; (ii) the

activation energy for the volume resistivity is much higher in the low temperature range and it decreases with increasing temperature; and (iii) the low-temperature activation energy decreases but the high-temperature activation energy increases with increasing yttria content.

Several different models have been proposed to explain the effect of temperature, dopant type and its concentration on the ionic conductivity and activation energy in materials with the fluorite-type structure.[23–27] In these systems, varying levels of interactions exist between dopant cations and vacancies. For dilute solid solutions simple associates may form, whereas for concentrated solution (large vacancy concentration) complex defect interactions involving several nearest neighbours can occur. At high temperatures where most of the vacancies are dissociated and free to migrate the activation energy equals the enthalpy of vacancy migration. The effect of cation size on conductivity and activation energy can be explained in terms of the steric blocking effect of the dopant cation.[28] A dopant cation with ionic radius larger than the host cation is likely to be more effective in hindering migration of vacancies and would give rise to higher activation energy and a lower conductivity. In the Sc_2O_3–ZrO_2 system, the cell volume decreases[29] and in the Y_2O_3–ZrO_2 system the cell volume increases[18] with increase in the dopant concentration. The ionic radius of Sc^{3+} is smaller and that of Y^{3+} is larger than that of Zr^{4+}. Thus the results in the high temperature range ($>850°C$) are consistent with the proposed hypothesis. Corman & Stubican[30] in the ternary system Y_2O_3–Yb_2O_3–ZrO_2 (total dopant content of 8 and 10 mol%) also observed a similar effect.

In the low temperature range, the activation energy, in addition to the enthalpy of vacancy migration, contains the binding energy term arising from interactions between dopant cations and vacancies. The binding energy is a combination of coulombic (charge, polarizability, etc., of the dopant cation) and strain (caused by different host and dopant cation sizes) energies. In this temperature range, although conductivity still decreases with increasing yttria content, the activation energy does not follow the high-temperature behaviour. In fact the results appear to suggest that the binding energy in the Sc_2O_3–ZrO_2 system is higher than that in Y_2O_3–ZrO_2. These results are consistent with those of Badwal[12,31] who reported much higher values for the conductivity as well as for the activation energy in 7·8 mol% Sc_2O_3–ZrO_2 compositions compared with 8 mol% Y_2O_3–ZrO_2 in the low-temperature region.

5 Conclusion

The conductivity in the ternary system Y_2O_3–Sc_2O_3–ZrO_2 was investigated for a constant dopant level of 8 mol%, because of the reported high ionic conductivity of scandia-doped zirconia and the ability of yttria to stabilize zirconia extremely well. The ternary compositions exhibited conductivity between those of binary systems. All the materials investigated were in the two-phase field. At 1000°C the initial conductivity of scandia-rich compositions was well above that reported for fully stabilized yttria–zirconia (FSZ $\approx 0{\cdot}1\ \Omega^{-1}\ cm^{-1}$). However, for all the compositions studied, the conductivity deteriorated with time at 1000°C. This results from the decomposition of the t′-phase for scandia-rich compositions to a dopant-rich cubic matrix and t-ZrO_2 precipitates. In yttria-rich compositions the conductivity deterioration occurs as a result of yttrium redistribution in the cubic phase and precipitation of t-ZrO_2. These results are consistent with the phase diagrams.[28,29] Even after extended annealing at 1000°C and despite considerable decrease in the conductivity, the final values obtained ($0{\cdot}1$–$0{\cdot}16\Omega^{-1}\ cm^{-1}$), especially for scandia-rich compositions, were still higher than that for FSZ.

Acknowledgements

The authors are thankful to Dr M. J. Bannister for reviewing this paper. The work reported in this paper formed part of FTC's M. App. Sci. at Chisholm Institute of Technology. He would like to thank his course supervisors Drs S. J. Bone and M. J. Bannister.

References

1. Etsell, T. H. & Flengas, S. N., The electrical properties of solid oxide electrolytes. *Chem. Rev.*, **70** (1970) 339–76.
2. Subbarao, E. C. (ed.), *Solid Electrolytes and Their Applications*. Plenum Press, New York, 1980.
3. Dell, R. M. & Hooper, A., Oxygen-ion conductors. *In Solid Electrolytes*, ed. P. Hagenmuller & W. van Gool. Academic Press, New York, 1978, pp. 291–312.
4. Williams, D. E. & McGeehin, P., Solid-state gas sensors and monitors. *Electrochemistry*, **9** (1984) 246–90.
5. Janke, D., Zirconia-, hafnia-, and thoria-based electrolytes for oxygen control devices in metallurgical processes. In *Advances in Ceramics, Vol. 3: Science and Technology of Zirconia I*. The American Ceramic Society, 1981, pp. 419–36.
6. Riley, B., Solid oxide fuel cells–the next stage. *J. Power Sources*, **29** (1990) 223–50.
7. Vayenas, C. G., Catalytic and electrocatalytic reactions in solid oxide fuel cell. *Solid State Ionics*, **28–30** (1988) 1521–39.

8. Isaacs, H. S., Zirconia fuel cells and electrolyzers. In *Advances in Ceramics, Vol. 3: Science and Technology of Zirconia I.* The American Ceramic Society, 1981, pp. 406–18.
9. Ciacchi, F. T., Badwal, S. P. S. & Drennan, J., The system Y_2O_3–Sc_2O_3–ZrO_2: Phase characterisation by XRD, TEM and optical microscopy. *J. Europ. Ceram. Soc.*, **7** (1991) 185–95.
10. Badwal, S. P. S. & Ciacchi, F. T., Performance of zirconia membrane oxygen sensors at low temperatures with nonstoichiometric oxide electrodes. *J. Appl. Electrochem.*, **16** (1986) 28–40.
11. Badwal, S. P. S., Ciacchi, F. T. & Ho, D. V., A fully automated four-probe DC conductivity technique for investigating solid electrolytes. *J. Appl. Electrochemistry*, in press.
12. Badwal, S. P. S., Effect of dopant concentration on electrical conductivity in the Sc_2O_3–ZrO_2 system. *J. Mater. Sci.*, **22** (1987) 4125–32.
13. Ioffe, A. I., Rutman, D. S. & Karpachov, S. V., On the nature of the conductivity maximum in zirconia-based solid electrolytes. *Electrochimica Acta*, **23** (1978) 141–2.
14. Kleitz, M., Bernard, H., Fernandez, E. & Schouler, E., Impedance spectroscopy and electrical resistance measurements on stabilized zirconia. In *Advances in Ceramics, Vol. 3: Science and Technology of Zirconia I.* The American Ceramic Society, 1981, pp. 310–36.
15. Badwal, S. P. S., Yttria tetragonal polycrystalline electrolytes for solid-state electrochemical cells. *Appl. Phys. A.*, **50** (1990) 449–62.
16. Vlasov, A. N. & Perfiliev, M. V., Ageing of ZrO_2-based solid electrolytes. *Solid State Ionics*, **25** (1987) 245–53.
17. Rossell, H. J. & Hannink, R. H. J., The phase $Mg_2Zr_5O_{12}$ in MgO partially stabilized zirconia. In *Advances in Ceramics, Vol. 12: Science and Technology of Zirconia II.* The American Ceramic Society, 1984, pp. 139–51.
18. Scott, H. G., Phase relationships in the zirconia–yttria system. *J. Mater. Sci.*, **10** (1975) 1527–35.
19. Stubican, V. S., Hink, R. C. & Ray, S. P., Phase equilibria and Ordering in the System ZrO_2–Y_2O_3. *J. Amer. Ceram. Soc.*, **61** (1978) 17–21.
20. Thornber, M. R., Bevan, D. J. M. & Summerville, E., Mixed oxides of the type MO_2 (fluorite)–M_2O_3. V. Phase studies in the systems ZrO_2–M_2O_3 (M = Sc, Yb, Er, Dy). *J. Solid State Chem.*, **1** (1970) 545–53.
21. Inozemstev, M. V., Perfil'ev, M. V. & Gorelov, V. P., Effect of annealing on the electrical and structural properties of electrolytes based on ZrO_2. *Sov. Electrochem.*, **12** (1976) 1128–32.
22. Moghadam, F. K., Yamashita, T., Sinclair, R. & Stevenson, D. A., Transmission electron microscopy of annealed ZrO_2 + 8 mol% Sc_2O_3. *J. Amer. Ceram. Soc.*, **66** (1983) 213–16.
23. Wang, Da. Yu., Park, D. S., Griffith, J. & Nowick, A. S., Oxygen-ion conductivity and defect interactions in Yttria-doped ceria. *Solid State Ionics*, **2** (1981) 95–105.
24. Kilner, J. A. & Waters, C. D., The effects of dopant cation–oxygen vacancy complexes on the anion transport properties of non-stoichiometric fluorite oxides. *Solid State Ionics*, **6** (1982) 253–9.
25. Hohnke, D. K., Ionic conduction in doped oxides with the fluorite structure. *Solid State Ionics*, **5** (1981) 531–4.
26. Nakamura, A. & Wagner, Jr, J. B., Defect structure, ionic conductivity, and diffusion in yttria stabilized zirconia and related oxide electrolytes with fluorite structure. *J. Electrochem. Soc.*, **133** (1986) 1542–8.
27. Kilner, J. A. & Brook, R. J., A study of oxygen ion conductivity in doped non-stoichiometric oxides. *Solid State Ionics*, **6** (1982) 237–52.
28. Stafford, R. J., Rothman, S. J. & Routbort, J. L., Effect of dopant size on the ionic conductivity of cubic stabilized ZrO_2. *Solid State Ionics*, **37** (1990) 67–72.
29. Bannister, M. J. & Skilton, P. F., The cubic⇌tetragonal equilibrium in the system zirconia–scandia at 1800°C: Effect of alumina. *J. Mater. Sci. Lett.*, **2** (1983) 561–4.
30. Corman, G. S. & Stubican, V. S., Phase equilibria and ionic conductivity in the system ZrO_2–Yb_2O_3–Y_2O_3. *J. Amer. Ceram., Soc.*, **68** (1985) 174–81.
31. Badwal, S. P. S., Effect of dopant concentration on the grain boundary and volume resistivity of yttria–zirconia. *J. Mater. Sci. Lett.*, **6** (1987) 1419–21.